DOI: 10.5327/Z2317-4889201400010007

ARTICLE

Paragenesis and evolution of the hydrothermal Bacuri iron oxide–copper–gold deposit, Carajás Province (PA)

Paragênese e evolução do depósito hidrotermal de óxido de ferro-cobre-ouro Bacuri, Província Carajás (PA)

Gustavo Henrique Coelho de Melo[1]*, Lena Virgínia Soares Monteiro[2], Carolina Penteado Natividade Moreto[1], Roberto Perez Xavier[1], Marco Antonio Delinardo da Silva[1]

ABSTRACT: The Bacuri copper deposit is located about 9 km east of the world-class Sossego iron oxide–copper–gold deposit in the Carajás Province. It is hosted by the *ca.* 2.84 Ga Serra Dourada granite, the Bacuri Porphyry, and subordinated gabbro. The Bacuri deposit is situated within the regional-scale, WNW-ESE-trending ductile Canaã shear zone, characterized by early albite, scapolite-magnetite, potassium feldspar and biotite-scapolite-magnetite hydrothermal alteration zones. Copper mineralization was controlled and largely simultaneous to the development of a NE-SW-trending transcurrent fault zone. Within this zone, intense chlorite alteration, silicification and quartz veining overlap previous hydrothermal stages. Copper ore (chalcopyrite-pyrite-magnetite) is disseminated and related to veins and breccias. Chalcopyrite occurs along the mylonitic foliation in chlorite alteration zones, in brecciated quartz-(muscovite-fluorite) and undeformed milky quartz veins and in late potassium feldspar-epidote veinlets with open space textures. The relative temporal history of the Bacuri deposit reveals significant changes in physico-chemical parameters during the system evolution. Contribution of hot hypersaline metalliferous fluids was important during early sodic and potassic alteration stages and related to a regional hydrothermal system developed at relatively deep crustal levels. Influx of externally derived diluted fluids within the NE-SW-trending fault zone favoured the late shallow-emplaced chlorite alteration and silicification, and may have triggered the ore deposition due to decrease of temperature and salinity, accompanied by fO_2 increase and pH decrease. Such significant changes could indicate a hybrid system that evolved in multiple pulses during progressive exhumation.

KEYWORDS: IOCG; metallogenesis; hydrothermal system; Neoarchean; Carajás Province.

RESUMO: *O depósito de cobre Bacuri está localizado a cerca de 9 km a leste da Mina Sossego, que representa um depósito de óxido de ferro-cobre-ouro de nível mundial da Província de Carajás. O depósito Bacuri é hospedado pelo Granito Serra Dourada de 2,84 Ga, pelo Pórfiro Bacuri, além de gabros, ao longo da Zona de Cisalhamento Canaã, regional, dúctil e de direção WNW-ESE. Essa zona regional caracteriza-se por alteração hidrotermal com albita, escapolita-magnetita e feldspato potássico, que evoluíram para zonas com biotita-escapolita-magnetita. A mineralização cuprífera foi controlada e simultânea ao desenvolvimento de uma falha transcorrente subsidiária de direção NE-SW, na qual alteração clorítica e silicificação se sobrepuseram aos estágios hidrotermais prévios. O minério cuprífero (calcopirita-pirita-magnetita) é disseminado e relacionado a veios e brechas. Calcopirita orienta-se ao longo da foliação milonítica na zona de alteração clorítica e preenche fraturas em veios brechados com quartzo-(muscovita-fluorita). Adicionalmente, é reconhecida em veios de quartzo tardios, indeformados, e em vênulas com feldspato potássico-epidoto, que apresentam texturas de preenchimento de espaços abertos. A evolução temporal do depósito Bacuri foi acompanhada por mudanças significativas nos parâmetros físico-químicos do sistema hidrotermal. Contribuição de fluidos metalíferos, hipersalinos e quentes foi importante nos estágios iniciais de alteração sódica e potássica desenvolvidos em níveis crustais mais profundos. Influxo de fluidos diluídos pode ter favorecido a deposição de minério devido à diminuição da temperatura e salinidade, que foi acompanhada por diminuição de pH e aumento de fO_2. Tais mudanças podem indicar um sistema hidrotermal híbrido que evoluiu em múltiplos pulsos durante sua progressiva exumação.*

PALAVRAS-CHAVE: *IOCG; metalogênese; sistema hidrotermal; Neoarqueano; Província Carajás.*

[1]Instituto de Geociências, Universidade Estadual de Campinas - Unicamp, Campinas (SP), Brazil. *E-mail: gustavodemelo@ige.unicamp.com; carolina.moreto@ige.unicamp.br; xavier@ige.unicamp.br; marco.silva@ige.unicamp.br*

[2]Instituto de Geociências, Universidade de São Paulo - USP, São Paulo (SP), Brazil. *E-mail: lena.monteiro@usp.br*

*Corresponding author

Manuscrito ID 30021. **Recebido em:** 14/08/2013. **Aprovado em:** 24/02/2014

INTRODUCTION

The Carajás Province (Santos *et al.* 2000), which was formed in the Mesoarchean and tectonically stabilized in the Neoarchean (Teixeira *et al.* 1989; Tassinari 1996; Tassinari & Macambira 1999), comprises the most ancient crustal nucleus in the south-eastern portion of the Amazonian Craton. It represents one of the most important mineral provinces in the world, standing out for its diversity and notable metallogenetic potential, including a broad range of deposits such as iron (e.g. N4, N5), iron oxide–copper–gold, manganese (e.g. Azul, Buritirama), nickel (e.g. Vermelho, Onça-Puma), chrome-PGE (e.g. Luanga), Au–Pd–Pt (e.g. Serra Pelada) and Cu–Mo–Au deposits (e.g. Serra Verde; Dardenne & Schobbenhaus 2001; Villas & Santos 2001).

In this scenario, the iron oxide–copper–gold (IOCG) deposits of Carajás represent an important target for the mineral industry. The main IOCG deposits at Carajás are Salobo (1.112 billion tonnes @ 0.69 wt.% Cu and 0.43 g/t Au; VALE 2012), Cristalino (500 Mt @ 1.0 wt.% Cu and 0.3 g/t Au; Huhn *et al.* 1999), Igarapé Bahia/Alemão (219 Mt @ 1.4 wt.% Cu and 0.86 g/t Au; Tallarico *et al.* 2005), Sossego (355 Mt @ 1.1 wt.% Cu and 0.28 g/t Au; Lancaster Oliveira *et al.* 2000), Alvo 118 (170 Mt @ 1.0 wt.% Cu and 0.3 g/t Au; Rigon *et al.* 2000) and other minor deposits (Castanha, Bacaba, Visconde, Jatobá and Bacuri) under evaluation by VALE mining company.

The Bacuri copper deposit is located approximately 9 km east from the world-class Sossego IOCG deposit, within an important regional ESE-WNW shear zone, subsidiary to the Canaã shear zone (Pinheiro *et al.* 2013). Despite its proximity to other important IOCG deposits, geological setting of the Bacuri copper deposit is poorly understood, especially the nature of its host rocks, paragenesis and relationship with a large hydrothermal system in the southern portion of the Carajás Domain. Similar paragenetic evolution (sodic and potassic alteration, magnetite formation, chlorite/epidote alteration, copper mineralization) has been recognized in the Sossego mine (Monteiro *et al.* 2008a) and in Cristalino, Alvo 118, Castanha, Bacaba, Visconde and Jatobá deposits (Augusto *et al.* 2008; Ribeiro 2008; Monteiro *et al.* 2011; Pestilho 2011; Craveiro *et al.* 2012; Torresi *et al.* 2012). However, the predominance of specific types of hydrothermal alterations and the distribution of alteration zones, which vary in each deposit, suggests distinct depth of formation (Hitzman *et al.* 1992; Williams *et al.* 2005) with variable proportion of magmatic and externally derived components in the paleohydrothermal systems.

In addition, new geochronological data for the Carajás IOCG deposits (*ca.* 2.71 – 2.68 Ga and 1.88 Ga; Moreto 2013) indicate that these deposits were not formed in a single metallogenetic event. Neoarchean and Paleoproterozoic events might be responsible for the complex puzzle of attributes of these important copper–magnetite deposits. Moreover, these data suggest that the Bacuri deposit is an example of a Neoarchean IOCG deposit in Carajás and may be part of a regional and protracted Neoarchean paleohydrothermal system.

This paper introduces the Bacuri deposit and aims to characterize its host rocks, distribution and types of hydrothermal alteration and ore typology and paragenesis, and to compare with the metallogeny of the IOCG deposits in the Carajás Province.

GEOLOGICAL SETTING OF THE CARAJÁS PROVINCE

The Carajás Province, located in the south-eastern part of the Amazonian Craton, is divided into two domains: Rio Maria, in the south, and Carajás, in the north (Vasquez *et al.* 2008), separated by an E-W regional shear zone (Fig. 1).

The basement in the Carajás Domain has been attributed to the Xingu Complex (2,974 ± 15 Ma; Machado *et al.* 1991), which includes tonalitic to trondhjemitic gneisses and migmatites, and to the Pium Complex with mafic granulites with crystallization age of 3,002 ± 14 Ma (U–Pb SHRIMP zircon; Pidgeon *et al.* 2000). Migmatization of the Xingu Complex (2,859 ± 2 Ma and 2,860 ± 2 Ma; U–Pb in zircon; Machado *et al.* 1991) and granulitization of mafic protoliths of the Pium Complex (2,859 ± 9 Ma; U–Pb in zircon; Pidgeon *et al.* 2000) were synchronic. Recent studies resulted in the individualization of other units assigned to the basement according to their distinct composition and ages in the southern sector of the Carajás Domain. These units include the Bacaba Tonalite and Sequeirinho Granite (*ca.* 3.0 Ga; U–Pb in zircon; Moreto *et al.* 2011; Moreto 2013); Canaã dos Carajás Granite (*ca.* 2.96 Ga); Rio Verde Trondhjemite (*ca.* 2.93 Ga); Campina Verde Tonalite (*ca.* 2.85 Ga) and Bom Jesus, Cruzadão and Serra Dourada granites (2.87 – 2.84 Ga; Moreto *et al.* 2011; Feio *et al.* 2013).

The basement rocks are overlain by the metavolcanosedimentary Rio Novo Group (*ca.* 2.76 Ga), which is composed of amphibolites, schists, metagreywackes, tholeiitic metavolcanic rocks and gabbros (Hirata *et al.* 1982), and the Itacaiúnas Supergroup (*ca.* 2.76 – 2.73 Ga; Wirth *et al.* 1986; DOCEGEO 1988; Machado *et al.* 1991).

The Itacaiúnas Supergroup was divided by DOCEGEO (1988) into four units designated as Igarapé Salobo, Igarapé Pojuca, Grão Pará and Igarapé Bahia groups. According to these authors, the Igarapé Salobo Group, which hosts the Salobo IOCG deposit, includes paragenesis, amphibolites,

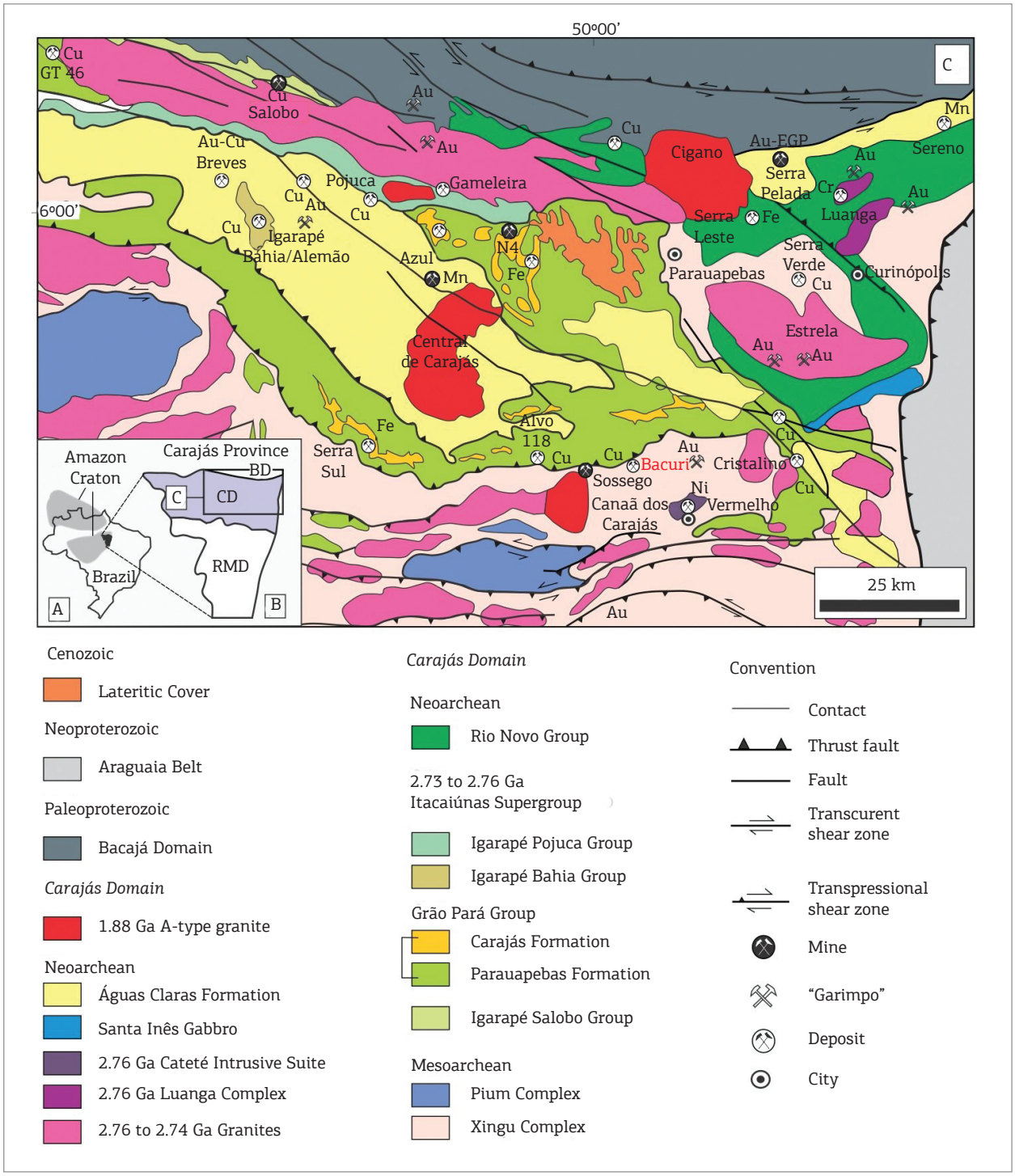

Figure 1. Geological map of the Carajás Domain and adjacent areas showing the distribution of the various IOCG deposits, including the Bacuri deposit (modified from Vasquez *et al.* 2008).

quartzites, metagreywackes and iron formation. The Igarapé Pojuca Group, which hosts the Gameleira IOCG deposit, is composed of basic metavolcanic rocks, schists and cordierite- and anthophyllite-bearing rocks. The Grão Pará Group, which hosts the outstanding giant iron deposits at Carajás, encompasses metabasalts, felsic metavolcanic rocks and jaspilites (*e.g.* Figueiredo & Silva *et al.* 2013). The Igarapé Bahia Group, which hosts the Igarapé Bahia/Alemão deposit, comprises metavolcanic, metapyroclastic and metasedimentary rocks metamorphosed in the greenschist facies, including iron formation.

The Águas Claras Formation overlaps, apparently in angular unconformity, the metavolcanosedimentary sequences of the Itacaiúnas Supergroup, and is composed of metaconglomerates,

metarenites, dolomitic marble, carbonaceous phillyte, and sericite quartzites. Their protoliths have been deposited in fluvial to shallow marine environment (Nogueira 1995), and a minimum age of deposition is given by the crystallization age of mafic dikes intrusive in this formation (2,708 ± 37 Ma; U–Pb in zircon; Mougeot *et al.* 1996).

Mafic-ultramafic layered intrusions represented by the Luanga Complex (*ca.* 2.76 Ga; Machado *et al.* 1991) host lateritic nickel, chrome and platinum group element mineralization.

The supracrustal sequences and the basement are cut by granitic intrusions: (i) *ca.* 2.76 – 2.73 Ga foliated syntectonic alkaline granites, comprising the Plaque, Planalto, Estrela, Igarapé Gelado and Serra do Rabo suites (Huhn *et al.* 1999; Sardinha *et al.* 2006); (ii) *ca.* 2.57 Ga peralkaline to metaluminous granitoids, represented by only two small granitic bodies, named Old Salobo and Itacaiúnas (Machado *et al*. 1991; Souza *et al*. 1996), which occur within the Cinzento Shear Zone; and (iii) *ca.* 1.88 Ga A-type alkaline to subalkaline granites, including the Central de Carajás, Young Salobo, Cigano, Pojuca, and Breves granites (Machado *et al.* 1991; Tallarico 2003).

Three main WNW-ESE shear zone systems have been characterized in the Carajás Domain, including Carajás and Cinzento in the north and Canaã in the south (Pinheiros *et al.* 2013). According to Pinheiro *et al.* (2013), the widespread E-W foliation, folding and faulting in the Carajás Domain were related to shortening from NNE to SSW. A major set of NE-SW sinistral strike-slip faults, analogous to R-type Riedel structures, were responsible for the sigmoidal "S-shape" of the Carajás Domain (Pinheiro *et al*. 2013).

IRON OXIDE–COPPER–GOLD DEPOSITS IN THE CARAJÁS PROVINCE: A BRIEF REVIEW

The Carajás Province has the highest concentration of high-tonnage IOCG deposits in the world (Monteiro *et al.* 2008a), which are located within or close to shear zones in the contact between the metavolcanosedimentary units of the Itacaiúnas Supergroup with the Mesoarchean basement rocks (Moreto *et al*. 2011).

In general, the Carajás IOCG deposits exhibit similar attributes, such as (i) strong spatial association with WNW-ESE shear zones and with minor subsidiary NE-SW faults; (ii) the presence of hydrothermal breccias; (iii) intense alkaline hydrothermal alteration; (iv) magnetite formation ensued by precipitation of sulphides and (v) a broad range of homogenization temperatures (100 – 570°C) and salinities (0 – 69 wt.% eq. NaCl) in fluid inclusions, pointing to fluid mixing that allowed the transport and precipitation of metals (Monteiro *et al.* 2008a; Xavier *et al.* 2012). Moreover, these deposits have significant contents of LREE (light rare earth elements), P, U, Ni, Co and Pd similar to those described in IOCG deposits in other provinces worldwide (Hitzman *et al.* 1992; Williams *et al.* 2005).

The IOCG deposits located in the northern part of the Carajás Domain, close to the contact with the Paleoproterozoic Bacajá Domain (Vasquez *et al.* 2008), show different host rocks, types and distribution of hydrothermal alteration zones and ore mineralogy in comparison with those of the deposits of the Southern Copper Belt (Moreto 2013). The Salobo deposit, the most important deposit in the north, has zones of intense potassic alteration with biotite and iron enrichment, including almandine, grunerite and fayalite, followed by magnetite formation in high temperatures and ductile conditions (Lindenmayer 2003; Melo *et al.* 2013). Ore minerals include chalcocite, bornite, chalcopyrite, and gold.

In the Southern Copper Belt (Moreto 2013), the IOCG deposits are located within the Canaã shear zone, a 20- to 14-km wide sinistral WNW-ESE shear zone that has been active in *ca.* 2.7 – 2.5 Ga (Pinheiro *et al.* 2013). These deposits show a paragenetic evolution including sodic, sodic-calcic and potassic alteration, magnetite formation, chlorite-epidote alteration, copper mineralization and late sericite alteration, which is similar to that identified in the Sossego mine (Monteiro *et al.* 2008a), Cristalino deposit (Ribeiro 2008) and others, such as Castanha, Bacaba, Visconde and Jatobá (Augusto *et al.* 2008; Monteiro *et al*. 2011; Pestilho 2011; Craveiro *et al*. 2012). However, the distribution of the hydrothermal alteration zones varies in each deposit. Alteration patterns similar to those developed in the deeper portions of IOCG systems, with predominance of albite-actinolite and apatite-magnetite associations, have been recognized in the Sequeirinho-Pista orebodies (Sossego mine). Meanwhile, hydrothermal assemblages typical of relatively shallow crustals levels, with predominance of K-feldspar, biotite, chlorite and sericite-hematite, are well developed in the Sossego orebody (Sossego mine) and the Alvo 118 deposit.

Geochronological studies do not support the synchronicity of genetic processes in the Carajás IOCG deposits. They allowed the identification of different metallogenetic events in the Archean [*ca.* 2.71 – 2.68 Ga (Moreto 2013) and 2.57 Ga (Réquia *et al.* 2003; Tallarico *et al.* 2005)] and the Paleoproterozoic [*ca.* 1.88 Ga (Tallarico 2003; Silva *et al.* 2005; Moreto 2013)], even in a single deposit (e.g. Sossego and Bacaba; Moreto 2013; Igarapé Cinzento, Silva *et al.* 2005).

The IOCG events have been interpreted as being connected to the widespread events of granite crystallization recognized in the Carajás Domain at *ca.* 2.76 – 2.73 Ga (e.g. Planalto, Plaque, Estrela, Igarapé Gelado) and *ca.* 1.88 Ga

(A-type granites). However, a minor magmatic event related to granite formation at *ca.* 2.57 Ga (e.g. Old Salobo Granite), restricted to the northern sector, was also considered responsible for the establishment of the Salobo and Igarapé-Bahia extensive hydrothermal–magmatic systems (Réquia *et al.* 2003; Tallarico *et al.* 2005), but still a matter of debate.

Boron (Xavier *et al.* 2008) and chlorine (Chiaradia *et al.* 2006) isotope studies point to the participation of both magmatic and externally derived basinal fluids for the Carajás IOCG systems. Stable isotopes and fluid inclusion studies also indicate fluid mixing involving an externally derived fluid (meteoric water or seawater) in the late stages of the hydrothermal systems evolution (Monteiro *et al.* 2008a; Xavier *et al.* 2012).

METHODS

Geological mapping in the vicinity of the Bacuri deposit area and systematic description of samples from five drill holes (BRID 02, 05, 07, 09 and 12) was accomplished, and samples representative of least altered, altered and mineralized lithotypes were collected. Detailed petrographic studies under transmitted and reflected light, and using scanning electron microscopy (SEM) coupled with EDS (energy-dispersive X-ray spectrometer) and cathodoluminescence, were carried out in the Geoscience Institute, University of Campinas, Brazil.

BACURI COPPER DEPOSIT: GEOLOGY AND HYDROTHERMAL ALTERATION

The Bacuri deposit (Figs. 2 and 3) is located within the WNW-ESE- trending regional Canaã shear zone and particularly in a NE-SW subsidiary transcurrent fault zone in the Mesoarchean basement, previously attributed to the Xingu Complex (DOCEGEO 1988; Machado *et al.* 1991). The host rocks comprise the Serra Dourada granite (*ca.* 2.84 Ga, U–Pb in zircon; Moreto *et al.* 2011; Feio *et al.* 2013; Figs. 4A and 4B), the Bacuri Porphyry (Figs. 4C and 4D) and gabbro dikes. All these lithotypes have been intensely modified by hydrothermal alteration and deformation.

Host rocks

The Serra Dourada granite (Moreto *et al.* 2011; Feio *et al.* 2013) is greyish-to-pinkish in colour, medium-to-coarse grained and predominantly isotropic (Fig. 4A) but locally foliated. It has subordinate pegmatitic (Fig. 4B) and micrographic facies and is cut by aplite dikes. Its average composition is represented by 35% quartz, 45% potassium feldspar and 20% plagioclase, as well as minor biotite, and it is classified as a syenogranite.

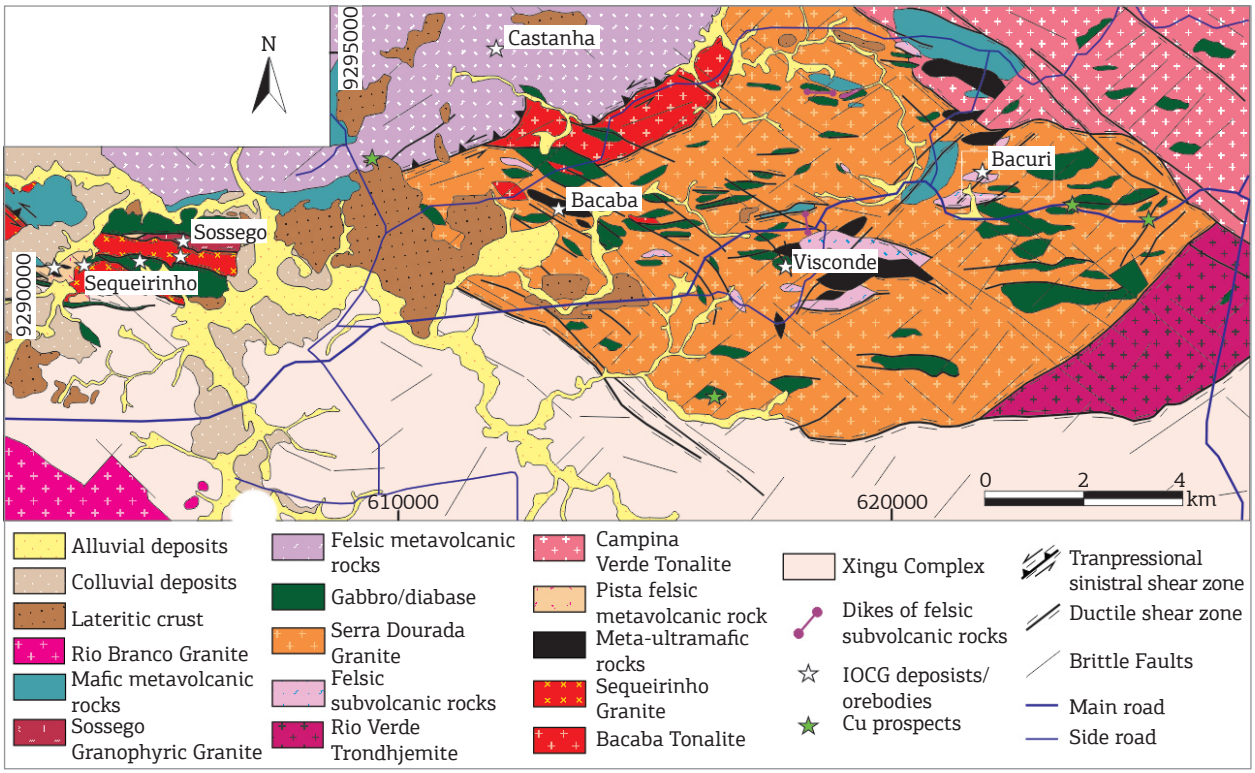

Figure 2. Geological map of the central west part of the Southern Copper Belt, in the Serra Dourada area, showing the location of Bacuri deposit (Moreto 2013).

The Bacuri Porphyry is intrusive in the Serra Dourada granite and represents the main host rock in the Bacuri deposit. Its occurrence is restricted to a NE-SW fault, and consequently, it is commonly strongly mylonitized, but locally relicts of igneous textures are recognized (Figs. 4C and 4D). In more preserved parts, the Bacuri Porphyry is grey, porphyritic and shows a fine-grained phaneritic matrix composed of quartz (> 50%), potassium feldspar (15%), plagioclase (20%), showing a dacitic composition. Idioblastic-to-subdioblastic phenocrysts of plagioclase (albite) (15%) are up to 3 mm long, show corrosion texture and are mostly fractured.

Gabbro dikes are dark green and have relicts of subophitic texture, defined by plagioclase laths and interstitial poikilitic augite. Late quartz-feldspar porphyry dikes with quartz and potassium feldspar phenocrysts cross-cut hydrothermal alteration zones and are only incipiently altered (Fig. 4E).

The host Serra Dourada granite, the Bacuri Porphyry and gabbro are strongly foliated within the NE-SW subsidiary transcurrent fault. These lithotypes show a NE-SW subvertical mylonitic foliation and evidence significant grain-size reduction in comparison with their least deformed protoliths. Ribbon structures and eye-shaped feldspar porphyroclasts are commonly present in the Bacuri Porphyry. In addition, the fine-grained matrix in these mylonites is predominantly composed of oriented hydrothermal minerals, re-crystallized quartz and intensely strained flattened grains of the pre-existing feldspar.

Hydrothermal alteration stages

Hydrothermal alteration in the Bacuri deposit is mainly controlled by the NE-SW subsidiary transcurrent fault zone, which represents the locus of the copper mineralisation. Outwards the fault zone, protoliths can still be recognized, and hydrothermal alteration mainly depends on the nature of rock (e.g. predominance of hydrothermal biotite in mafic rocks and potassium feldspar in felsic host rocks). In proximal zones, pre-existing features of the host rocks are predominantly obliterated and different protoliths develop similar hydrothermal paragenesis.

Early alteration stages are also mainly identified in the distal portions of the deposit. In proximal zones, overprinting of late pervasive alteration stages and telescoping prevail.

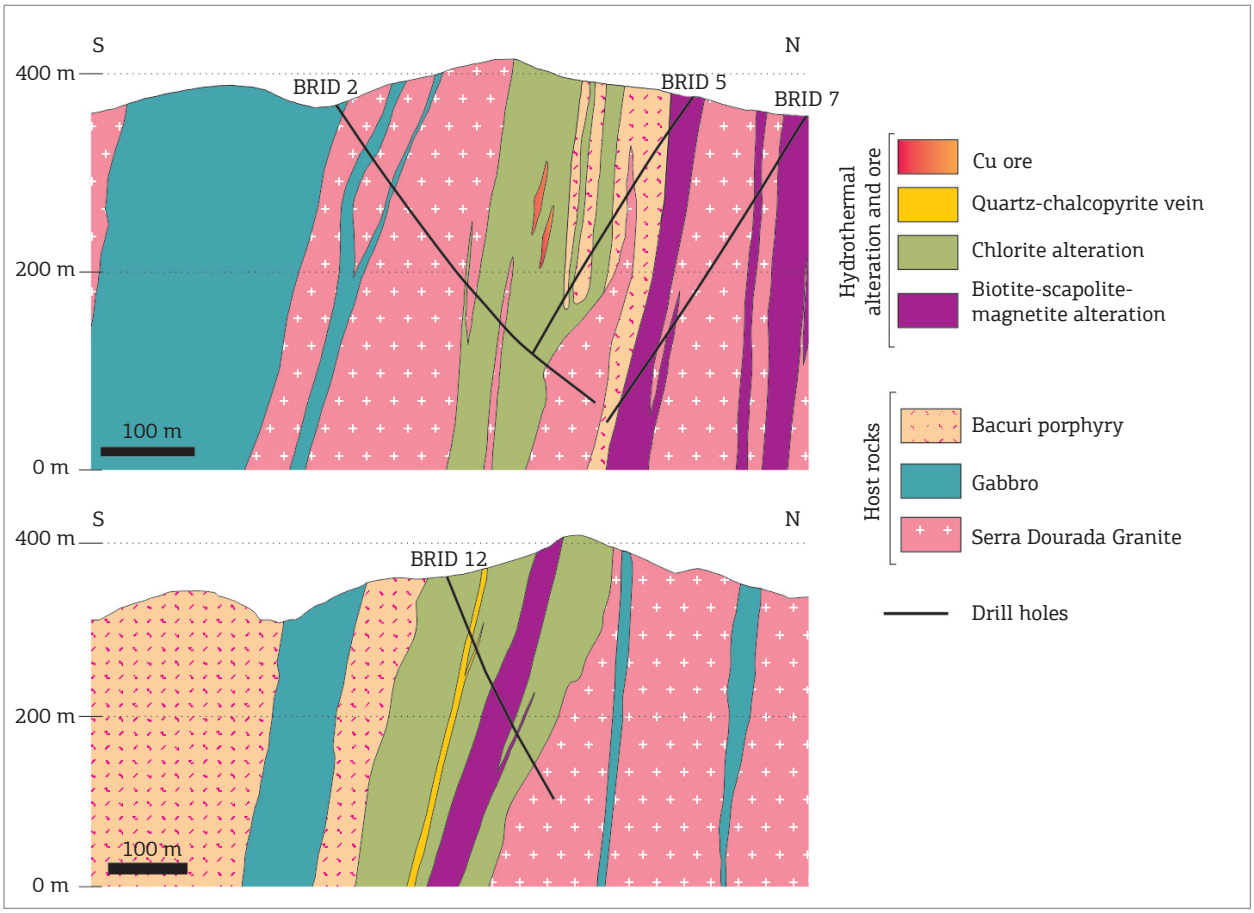

Figure 3. Schematic geological profiles of the Bacuri deposit, showing host rocks, main hydrothermal alteration zones, and orebodies related with chloritic zones and quartz veins (modified from VALE 2009).

However, a complete succession of hydrothermal alteration stages in the Bacuri deposit (Fig. 5) can be revealed by temporal relationships among hydrothermal mineral phases, such as cross-cutting zones, replacement haloes and remnants of previous hydrothermal assemblages within later alteration zones observed in both distal and proximal zones.

In distal zones, the Serra Dourada granite is the predominant host rock. It mainly shows early pervasive sodic alteration with albite and minor scapolite, which replaces the igneous potassium feldspar and plagioclase respectively. The sodic alteration is overprinted by potassic alteration with potassium feldspar and biotite. Chlorite alteration is incipient in the distal alteration zones within the Serra Dourada granite and occurs especially in a fissural style, selectively replacing biotite crystals. Muscovite formation is late and occurs as external haloes in relation to chalcopyrite-bearing quartz-(feldspar-muscovite) veins. Pervasive silicification and quartz veining are also recognized. The latter was accompanied by chalcopyrite and muscovite formation in late stages. In these distal zones, gabbro has also evidence of hydrothermal alteration although subophitic texture is preserved. Scapolite is recognized on the rims of the igneous plagioclase crystals and in veinlets. Augite was successively replaced by hastingsite, biotite and chlorite.

In proximal zones, the main lithotype is represented by the Bacuri Porphyry, but the Serra Dourada granite and gabbro are also recognized. A similar paragenetic sequence to that of the Serra Dourada granite in distal zones is observed; however, hydrothermal alteration is more intense and pervasive, resulting in extremely modified lithotypes. Zones with hydrothermal biotite-scapolite and chlorite are the most predominant.

Late dikes of quartz-feldspar porphyry, even in proximal zones, cross-cut intensely altered rocks but have only epidote veins and narrow haloes with potassic feldspar. The types of hydrothermal alteration identified in the Bacuri deposit are detailed below.

EARLY ALBITE ALTERATION

Formation of albite (I) corresponds to the initial stage of sodic hydrothermal alteration of the Bacuri deposit and results in white-to-pinkish colour in altered portions of the Serra Dourada granite (Figs. 6A and 6B) and Bacuri Porphyry in distal zones of the deposit (Fig. 6C). Hydrothermal albite (I) with chessboard texture (Fig. 6E) either selectively replaces the igneous potassium feldspar in the Serra Dourada granite or fills veinlets.

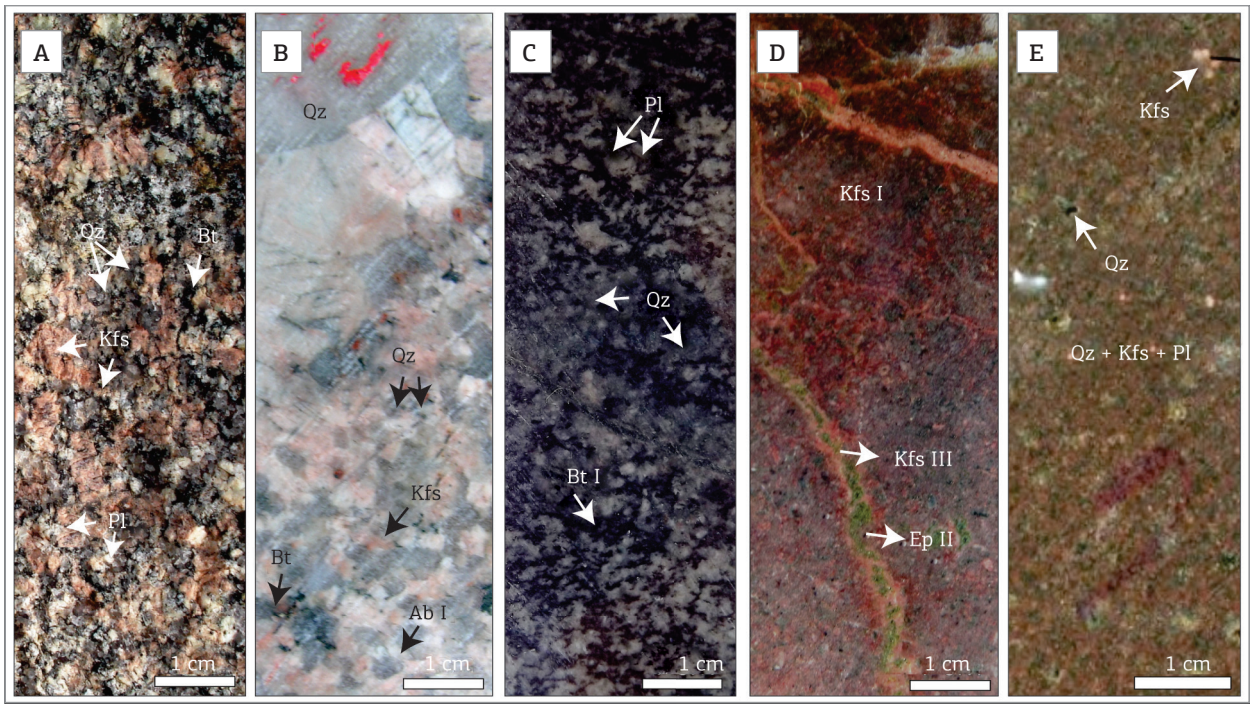

Figure 4. (A) Isotropic facies of the Serra Dourada granite in the outskirts of the Bacuri deposit, without any evidence of hydrothermal alteration; (B) Pegmatitic facies of the Serra Dourada granite. (C) Typical texture of the Bacuri Porphyry in the drill cores of Bacuri deposit, showing a quartz-feldspathic matrix with hydrothermal biotite in the interstices. (D) Hydrothermally altered Bacuri Porphyry with pervasive potassic alteration with potassium feldspar (I) and late veinlets of epidote (II) and potassium feldspar (III). (E) Quartz-feldspar porphyry with quartz and potassium feldspar phenocrysts.

SCAPOLITE-(MAGNETITE) ALTERATION AND VEINING

The Bacuri deposit records an intense and widespread process of scapolite formation, recognized in the distal and proximal alteration zones. In distal zones, the early scapolite (I) replaces igneous plagioclase along their crystals edges and cleavage planes (Fig. 6F) in the Serra Dourada granite and gabbro and also occurs in the quartz–feldspathic matrix of the Bacuri Porphyry. Veinlets infilled by scapolite (I) are also common.

Towards the central zone of the deposit, scapolite (+magnetite I±quartz) veins up to 10 cm are also observed. In these veins, scapolite (I) crystals are coarse-grained (up to 2-mm long), are fibrous, and show undulose extinction and subgrain formation. Fibrous scapolite (I) is cross-cut by fine-grained scapolite (II) crystals in deformed portions of the veins. All scapolite generations have low birefringence under polarized transmitted light, indicating marialite composition [$Na_4(AlSi_3O_8)_3(Cl_2,CO_3,SO_4)$] with low meionite content. Magnetite (I) is strongly related to scapolite alteration and occurs as tiny crystals in the edges and as inclusions in scapolite crystals in veins.

Evidence of scapolite replacement by later hydrothermal mineral phases is commonly observed. Network of biotite veinlets cross-cuts scapolite crystals, which are also replaced by potassium feldspar, and thereafter, by fine-grained muscovite.

POTASSIC ALTERATION WITH POTASSIUM FELDSPAR

The potassic alteration stage with potassium feldspar is selective in the Serra Dourada granite and pervasive in the Bacuri Porphyry, giving a reddish colour to the altered rock (Figs. 6A, 6B and 6D). In both lithotypes, hydrothermal potassium feldspar (I) replaces igneous microcline and plagioclase, and hydrothermal scapolite. The hydrothermal feldspar is characterized under microscope for examining its turbidity and lack of twinning. Generally, the pervasive potassic alteration zones with potassium feldspar (I) are cross-cut by biotite veinlets. Potassium feldspar is replaced by late fine-grained muscovite and/or chlorite as well.

BIOTITE-(SCAPOLITE-MAGNETITE) ALTERATION

Incipient potassic alteration with biotite is recognized in least-altered Serra Dourada granite and Bacuri Porphyry, and is characterized by biotite (I) crystals primarily in veinlets and in the interstices of the igneous quartz–fedspathic matrix of both host rocks. Biotite is also commonly observed in altered gabbro, mainly replacing augite.

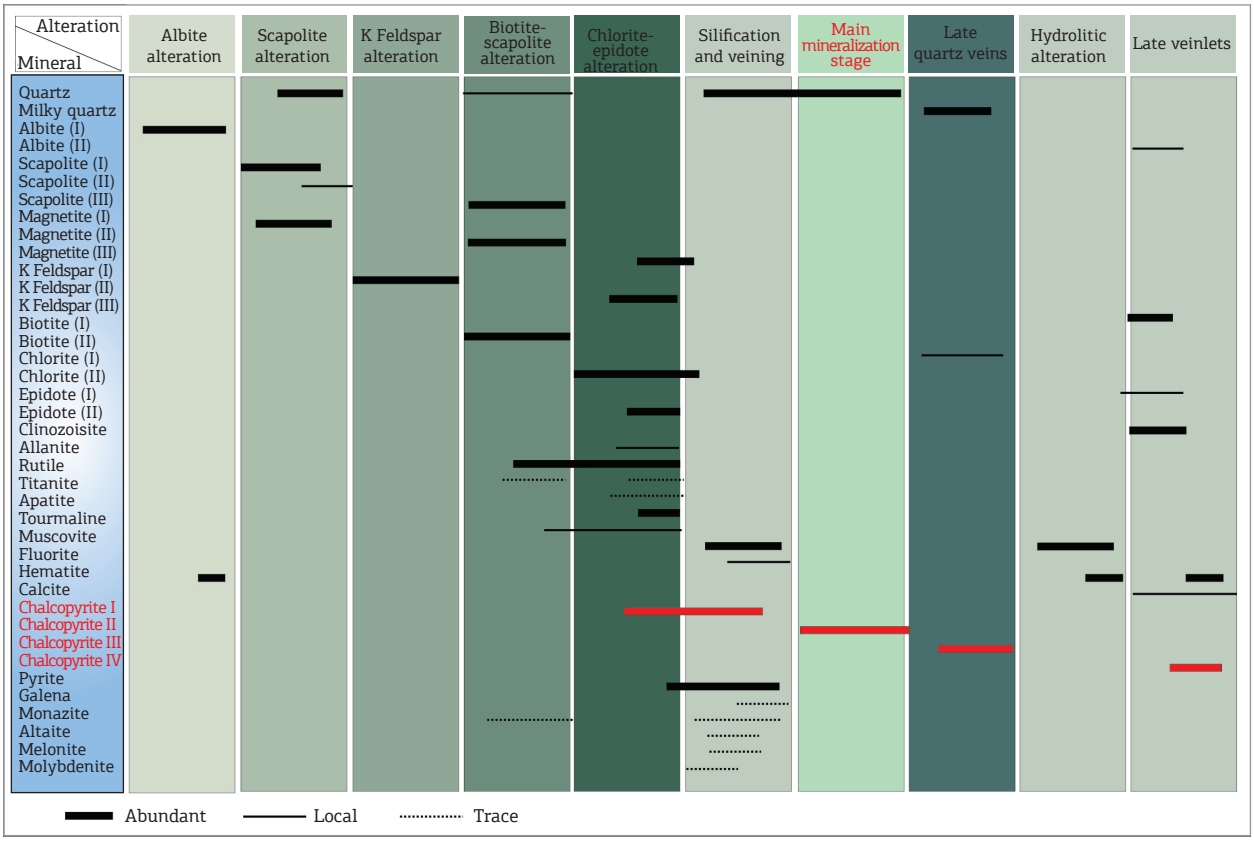

Figure 5. Paragenetic evolution of the Bacuri hydrothermal system.

In proximal zones, biotite-scapolite alteration grades from selective and fissural to pervasive (Fig. 6D) and obliterates the protolith features (Fig. 6G). The mineral assemblage identified in these zones includes biotite (I) + scapolite (III) ± magnetite (II) ± quartz ± allanite ± monazite ± fluorite ± rutile. The altered rocks commonly show mylonitic foliation and are grey-to-brown in colour due to the predominance of biotite (I), but white spots represented by scapolite crystals are very common (Fig. 7A). Mylonitic foliation is defined by the orientation of hydrothermal fine-grained biotite crystals and stretched quartz crystals (Fig. 7C), which show undulose extinction and subgrain formation. Scapolite (III) crystals are deformed and commonly have pressure shadows. Network of scapolite veinlets is also recognised in the biotite-scapolite alteration zones.

A second generation of magnetite is broadly found in the scapolite-biotite rich rocks. Magnetite (II) occurs as subdioblastic to idioblastic crystals disseminated in the rock and concordant to the mylonitic foliation. A fair increase in the size of magnetite crystals is accompanied by an increase in the biotite amount. In strongly mylonitized zones, deformed magnetite crystals are variably martitized and occur associated with tabular hematite crystals.

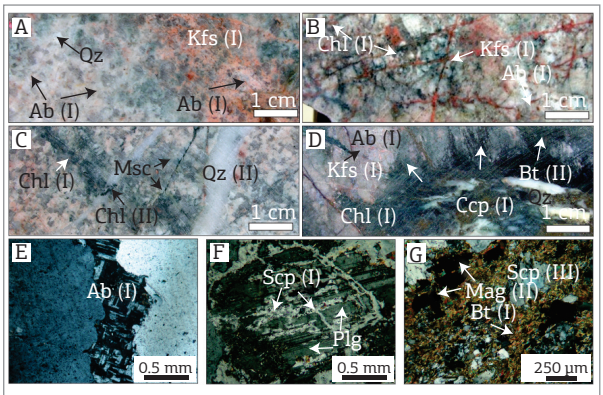

Ab = albite; Bt = biotite; Chl = chlorite; Ccp = chalcopyrite; Kfs = potassium feldspar; Mag = magnetite; Ms = muscovite; Qz = quartz; Scp = scapolite.

Figure 6. (A) Early albite (I) alteration in the Serra Dourada granite overprinted by potassium feldspar (I) alteration. (B) Zones of intense albite alteration in the Serra Dourada granite with veinlets of potassium feldspar (I) and chlorite (I). (C) Narrow zone with chlorite alteration cross-cut by milky quartz-(chlorite II) veinlet in the Serra Dourada granite. (D) Remains of sodic alteration with pinkish albite (I) in the Bacuri Porphyry overprinted by fronts of potassic alteration with biotite, which evolved to chlorite alteration with quartz and chalcopyrite (I). Fine veinlets with potassium feldspar (II) also cross-cut zones with albite (I). (E) Hydrothermal albite (I) showing chessboard texture in the Serra Dourada granite. (F) Selective scapolite alteration along the cleavage planes of plagioclase in the Serra Dourada granite. (G) Scapolite (III)-biotite (I) alteration zone in the Bacuri Porphyry associated with magnetite (II). Photos E–G are polarized light images.

CHLORITE-(EPIDOTE) ALTERATION AND VEINING

Chlorite alteration is the most common and well-developed alteration in the host rocks of the Bacuri deposit and is strongly controlled by the NE-SW fault zone development.

In the distal zones, chlorite (I) replaces the biotite (I) crystals (Fig. 6D), or it occurs in veinlets and interstices of igneous crystals, in the Serra Dourada granite and mainly in the Bacuri Porphyry (Figs. 7B and 7C).

Towards the orebodies, amount and size of chlorite veinlets increase and the chlorite alteration grades to pervasive. In intensely altered zones, there is a complete replacement of all igneous minerals by aggregates of fine-grained chlorite crystals (Figs. 7D, 7E and 7K). Chlorite alteration accompanies the increased intensity of the mylonitisation of the host rocks, resulting in strongly foliated rocks composed mainly of chlorite.

The common mineral association in this stage is represented by chlorite (I) + potassium feldspar (II) + magnetite (III) ± chalcopyrite (I) ± quartz ± epidote-group minerals ± apatite ± tourmaline ± monazite ± titanite. The potassium feldspar (II) was characterized using mainly EDS. It occurs strictly surrounding or near chalcopyrite, magnetite (III) and epidote crystals in chlorite mylonites, and is clear and limpid under transmitted light (Fig. 7E).

Tourmaline occurs in clusters of idioblastic crystals, which are recognized in very limited portions of the rock within the fronts of chlorite alteration and copper mineralisation. Tourmaline has strong pleochroism under transmitted light from dark blue to light blue or greyish, whose composition and optical properties are compatible with schorl (Fig. 7I).

Epidote-group minerals, such as epidote (I), clinozoisite and allanite are specially associated with chlorite, potassium feldspar (II) and chalcopyrite. They are observed disseminated parallel to the foliation and in veinlets.

SILIFICATION AND QUARTZ VEINING

Pervasive silicification and hydrothermal quartz veins cross-cut and are overprinted by the same hydrothermal alteration assemblage, indicating recurrence of silicification and veining. In distal zones of the deposit, silicification is less intense and mostly associated with biotite-scapolite alteration (Fig. 7C). Although quartz veins are recognized in distal zones, fronts of silicification predominate.

In the proximal zones to ore, the host rocks are cut by quartz (I) veins and replaced by subdioblastic quartz (I) crystals up to 2 cm long (Figs. 8D and 8E) in irregular alteration fronts and pockets. Quartz (I) crystals in silicified zones and in early veins are strongly deformed, showing undulose extinction, subgrain formation and ribbons (Fig. 7L), and the veins are brecciated. Coarse-grained flaky muscovite crystals (Fig. 7M) with kink bands, fluorite and chalcopyrite (II) are common in brecciated quartz veins (Fig. 7G).

Late milky quartz (II) veins (Figs. 8B and 8E) with chalcopyrite (III) and minor chlorite commonly cross-cut the chlorite mylonites and brecciated quartz veins of previous generations. Coarse-grained (up to 0.5 cm long) biotite (II) crystals befringe late quartz veinlets.

HYDROLYTIC ALTERATION

Hydrolytic alteration is represented by a large amount of greenish-to-whitish flakes of fine-grained muscovite associated with hematite, which replace previous potassium feldspar, albite and biotite. Close to deformed quartz veins, haloes with coarse-grained muscovite are also observed.

LATE EPIDOTE VEINING

Zoned veins and veinlets with open-space filling textures cross-cut zones with biotite-scapolite, chlorite (Fig. 7E) and even hydrolytic alteration. In these late veins, epidote (II), potassium feldspar (III), chalcopyrite (IV), calcite, chlorite (II) and albite (II) form crystals up to 3 mm long. Potassium feldspar (III) crystals are cloudy, differing from the clear potassium feldspar (II), and albite occurs as euhedral crystals.

CARBONATE VEINS

Late calcite-(hematite) crystals (Fig. 7H) are observed in veinlets of approximately 2 mm in width that cross-cut zones of previous stages of hydrothermal alteration. Thin calcite veinlets cut even the quartz-muscovite and milky quartz veins (Fig. 7N).

Characterization of the Copper Ore

The orebodies are represented by small lenses, veins and breccia bodies, which are spatially related to a NE-SW-striking transcurrent fault. Copper mineralisation is recognized in (i) chlorite-(epidote) alteration zones, (ii) brecciated silicified zones and deformed quartz-(muscovite-fluorite) veins, (iii) undeformed milky quartz veins and (iv) late zoned potassic feldspar-epidote veinlets.

In the chlorite–epidote alteration zones, the copper mineralisation is expressive and represented by disseminated chalcopyrite crystals, which are stretched and oriented along the mylonitic foliation (Figs. 8A and 8H). Chalcopyrite (I) is surrounded by clear potassium feldspar (II) (Figs. 8I and 8L) and, locally, infills fractures in hydrothermal apatite (Fig. 8K). Magnetite (III) and pyrite (Fig. 8G) are associated with chalcopyrite in centimetre-wide mineralised pockets. Andradite occurs as idioblastic inclusions in chalcopyrite crystals (Fig. 8J). Melonite ($NiTe_2$), altaite (PbTe), galena and cheralite [$CaTh(PO_4)_2$] occur as tiny inclusions in chalcopyrite crystals that can be identified only with the use of SEM.

However, the main orebodies are related to brecciated silicified zones and deformed quartz-(muscovite-fluorite) veins (Figs. 8A, 8C and 8D) within zones of intense chlorite alteration. Chalcopyrite (II) and pyrite not only commonly infill network of fractures in deformed quartz and cleavage planes of muscovite, but are also concentrated in massive sulphide zones that replace the brecciated silicified rock.

Chalcopyrite (III) is also observed in late milky quartz veins (Fig. 8E) and in veinlets with cloudy potassium feldspar (III; Figs. 8F, 8G and 8H) and epidote (II). The latter show comb and open-space filling textures characterized by crustiform or symmetrical banding.

Malachite [$Cu_2CO_3(OH)$] represents the supergene copper-rich mineral phase, which appears at surface in the chlorite mylonites and in quartz veins.

DISCUSSION

The Bacuri deposit is located within the regional ESE-WNW Canaã shear zone where several IOCG deposits (e.g. Sossego, Cristalino, Bacaba, Castanha, and Jatobá) are also known to exist. However, the deposit is closely related to a NE-SW-trending subsidiary transcurrent fault, which represents a local structural control on copper mineralisation. The Bacuri deposit is hosted by the *ca.* 2.84 Ga Serra Dourada granite (Moreto *et al.* 2011; Feio *et al.* 2013), the Bacuri Porphyry and subordinated gabbro dikes. The least-altered Serra Dourada granite is predominant in the distal parts of the deposit, whereas the Bacuri Porphyry represents the main lithotypes within the NE-SW-trending fault. All host rocks are mylonitized and show intense hydrothermal alteration.

Spatial zoning of hydrothermal alteration has been characterized in the Bacuri deposit. In distal zones, a regional halo of incipient sodic (albite and scapolite-magnetite) alteration overprinted by fissural potassic alteration with potassic feldspar or biotite prevails. Hydrothermal alteration in distal zones was predominantly controlled by the nature of

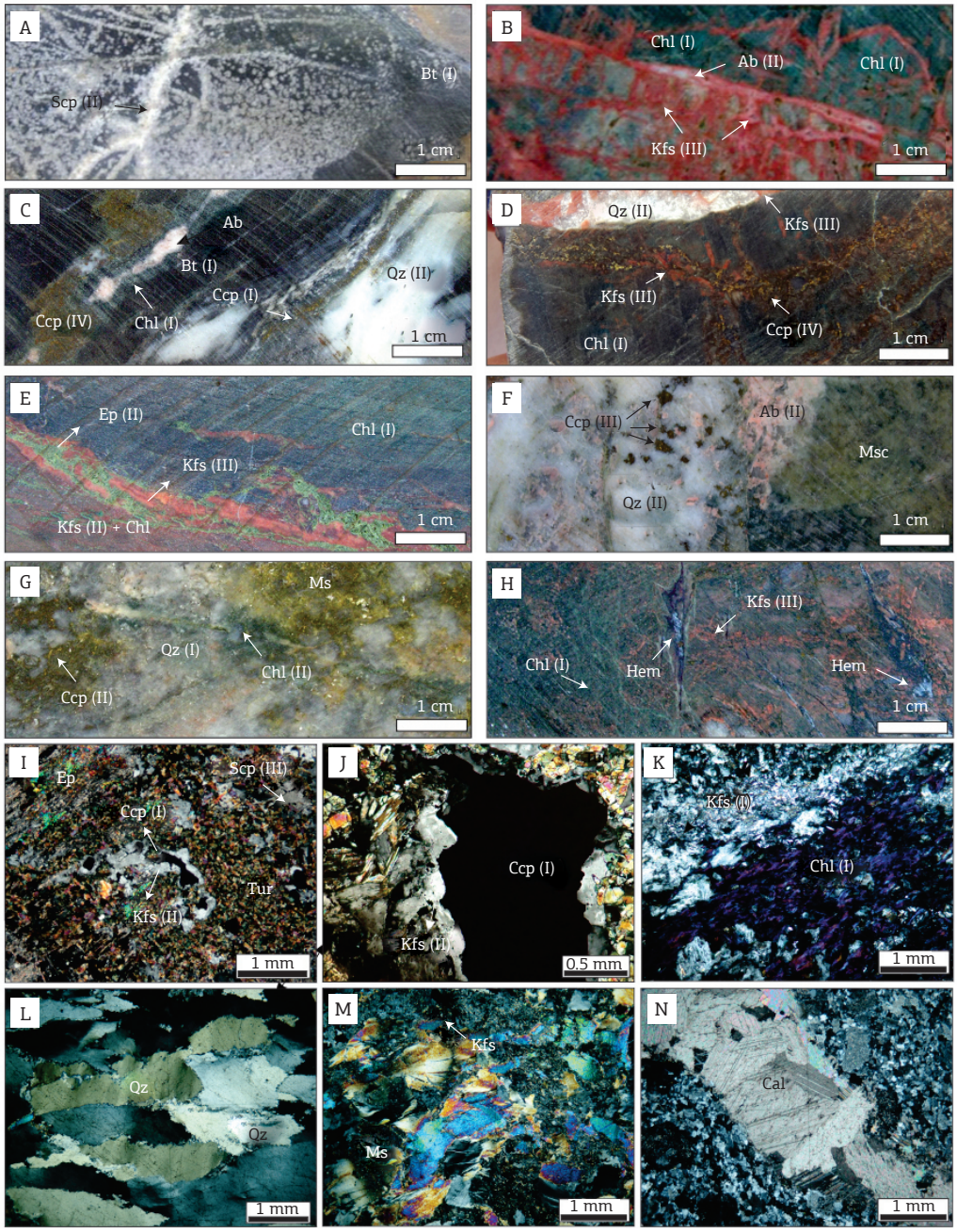

Ab = albite; Bt = biotite; Cal = calcite; Chl = chlorite; Czo = clinozoisite; Ccp = chalcopyrite; Ep = epidote; Hem = hematite; Kfs = potassium feldspar; Mag = magnetite; Ms = muscovite; Qz = quartz; Scp = scapolite; Tur = tourmaline.

Figure 7. (A) Scapolite veinlets and replacement zones in biotite–scapolite alteration zones in the Bacuri Porphyry. (B) Late potassic feldspar (III)-albite (II) veinlets cross-cut the chlorite-altered Bacuri Porphyry. (C) Biotite-(scapolite) alteration zone partially replaced by the association of chlorite (I)-quartz-chalcopyrite (I)-albite along the mylonitic foliation. (D) Veinlets of potassium feldspar (III) with chalcopyrite (IV) in zones of intense chlorite alteration. (E) Chlorite mylonite cut by potassium feldspar (III)-epidote (II) veins. (F) Replacement of hydrothermal biotite by fine-grained muscovite close to quartz vein with chalcopyrite in the Serra Dourada granite. (G) Veinlets of late chlorite (II) cross-cutting previous zones of muscovite and chalcopyrite. (H) Hematite-calcite veinlets cross-cutting veinlets of potassic feldspar (III) in chlorite alteration zone developed in the Bacuri Porphyry. (I) Tourmaline crystals associated potassium feldspar (II), epidote and chalcopyrite. (J) Chalcopyrite in paragenesis with clear potassium feldspar (II) that surrounds the chalcopyrite. (K) Zones of intense chlorite alteration concordant to the foliation and associated with potassic alteration (II). (L) Silicification with deformed quartz showing undulose extinction and subgrain formation. (M) Feldspar crystals strongly altered by fine-grained muscovite, associated with coarse-grained deformed muscovite crystals with kink bands. (N) Calcite veinlet cross-cutting the Bacuri Porphyry. Photos I–N are polarised light images.

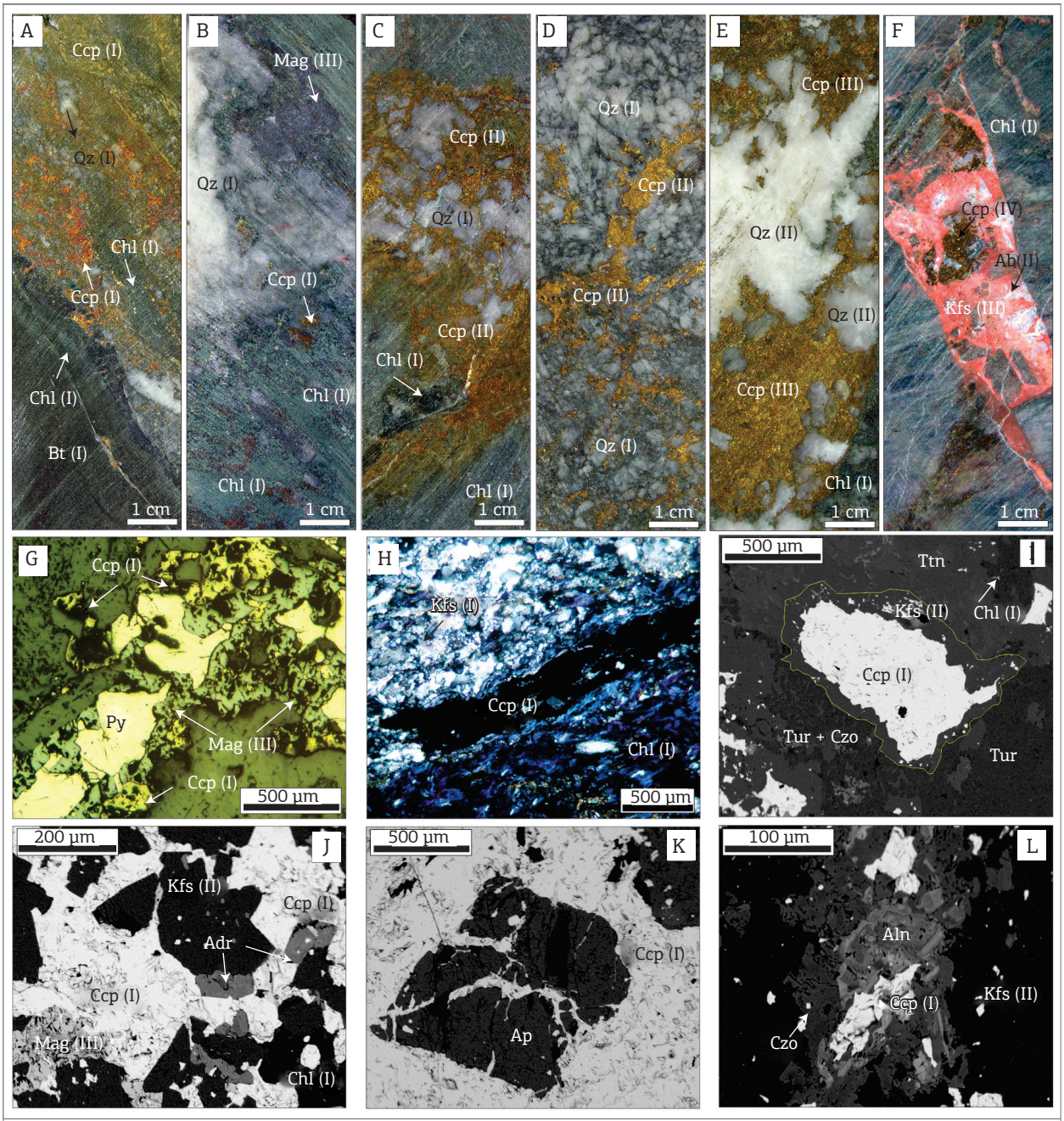

Ab = albite; Aln = allanite; Ap = apatite; Bt = biotite; Chl = chlorite; Czo = clinozoisite; Ccp = chalcopyrite; Ep = epidote; Kfs = potassium feldspar; Mag = magnetite; Ms = muscovite; Py = pyrite, Qz = quartz; Scp = scapolite; Ttn = titanite; Tur = tourmaline.

Figure 8. (A) Chlorite (I) alteration with chalcopyrite (I) and quartz along foliation and relicts of the previous biotite (I). (B) Chlorite alteration zone with silicification, magnetite (III) and minor chalcopyrite (I). (C) Replacement zone with chalcopyrite (II) and quartz in chlorite mylonite. (D) Brecciated silicified zones with infill of chalcopyrite (II) in fractures. (E) Chalcopyrite (III) associated with late milky quartz. (F) Late potassic feldspar (III)-chalcopyrite (IV)-calcite veins in chlorite mylonite. (G) Thin veinlets of chalcopyrite-pyrite-magnetite in the chlorite alteration zone (photomicrographs under reflected light). (H) Stretched chalcopyrite (I) crystals within chlorite alteration zone (polarized transmitted light). (I) Chalcopyrite (I) surrounded by potassium feldspar (II) with associated tourmaline, clinozoisite, chlorite and minor titanite (backscattered electron image). (J) Chalcopyrite (I) with inclusions of magnetite (III), andradite, potassium feldspar (II) and chlorite (I). (K) Idioblastic apatite crystal cross-cut by fractures filled with chalcopyrite (I) (backscattered electron image). (L) Chalcopyrite (I) surrounded by clinozoisite, allanite and potassium feldspar (II) (backscattered electron image).

host rocks, indicating relatively low fluid/rock (W/R) ratios. In proximal zones to ore, within the fault zone, pervasive chlorite alteration, in addition to silicification and quartz veining, is ubiquitous. The nature of host rocks was obliterated and distinct protoliths developed similar hydrothermal paragenesis, which points to high W/R ratios.

The NE-SW subsidiary fault likely played a fundamental role in the formation of the deposit as an effective pathway for fluid circulation, which promotes intense fluid–wall rock interaction. However, if all the hydrothermal alteration stages were related to a single fluid pulse, the expected spatial zoning would reveal a sequence of alteration mineral assemblages that advances outward from the main fluid conduit (Reed 1997). Thus, the latest alteration stages would be found in distal zones. In the Bacuri deposit, however, a more complex sequence of alteration was characterized, implying overprinting of multiple fluid pulses or telescoping.

The characterisation of the relative temporal history of the Bacuri deposit also reveals significant changes in physico-chemical parameters during the system evolution. The early hydrothermal stage, preserved mainly in the Serra Dourada granite in distal parts of the Bacuri deposit, is represented by the incipient sodic alteration, characterized by the replacement of the igneous potassium feldspar or plagioclase by hydrothermal chessboard albite. Sodic alteration also resulted in scapolite-(magnetite) formation in (i) veins and veinlets, in which fibrous scapolite (I) and associated magnetite (I) formed directly from the hydrothermal fluid; and (ii) altered rock (e.g. Serra Dourada granite, Bacuri Porphyry and gabbro), as replacement of previous igneous minerals due to mechanisms of fluid–rock interaction (diffusion, dissolution and re-precipitation). Scapolite (I) crystals in veins show undulose extinction and subgrain formation, evidencing deformation posterior or simultaneous to its formation.

Scapolite (I) and (II) in veins and altered rocks has low birefringence under polarized transmitted light, indicating marialitic composition [$Na_4(AlSi_3O_8)_3(Cl_2,CO_3,SO_4)$] with low meionite content. Scapolite with marialitic composition is considered as a key mineral indicator of chlorine content in fluids (Vanko & Bishop 1982). In addition, as chlorine is strongly partitioned into fluids in relation to solid phases, chlorine-bearing minerals, such as scapolite, may be a particularly sensitive indicator of fluid–rock interaction and mixing with external fluids (Mora & Valley 1989). The marialite occurrence in the Bacuri deposit reflects temperatures over 500 – 400°C (Vanko & Bishop 1982) and buffering of chlorine activity in the early stages of evolution of the hydrothermal system. This could be attributed to regional migration of hypersaline brines without infiltration of diluted fluids, favouring metal (copper, iron, gold) leaching from host rocks and their transport as chlorine complexes.

The precipitation of sodium-bearing minerals (e.g. albite and scapolite) increased the potassium activity in the fluid, allowing the development of zones of potassic alteration with potassium feldspar, which are recognized in the Serra Dourada granite and the Bacuri Porphyry. The precipitation of potassium feldspar was ensued by pervasive and intense biotite (I)-scapolite (III)-magnetite (II) alteration. The presence of scapolite in this mineral association indicates that hypersalinity of fluids still prevailed during the biotite-scapolite-magnetite stage. Fluctuations of fO_2 conditions due to fluid–rock interaction likely controlled the formation of biotite instead of potassium feldspar in this stage.

In the biotite-scapolite-magnetite alteration zones, biotite is oriented parallel to the mylonitic foliation and scapolite crystals are deformed and show pressure shadows. These relationships may suggest that scapolite was formed before the shearing and biotite may have been re-oriented.

Chlorite alteration is the main hydrothermal stage in the Bacuri deposit, overlapping all previous ones. Chlorite alteration is pervasive and resulted in chlorite formation in paragenesis with magnetite (III), epidote (I), apatite, allanite, clinozoisite and monazite, especially in proximal zones close to the orebodies. The overprinting of biotite-scapolite-magnetite zones by the chlorite alteration shows decrease of pH conditions (Fig. 9). Destabilisation of scapolite in this stage may have been favoured by influx of external diluted fluids.

Significant silicification and quartz veining that accompanied and followed the chlorite alteration also suggest significant physico-chemical gradients. As the silica solubility decreases with decreasing salinity, temperature and pH (Fournier 1983), these parameters may have controlled quartz deposition. Silicification and veining were likely strongly influenced by mixing of high- and low-salinity solutions, once mixing promotes significant quartz precipitation (Rimstidt 1997). In early deformed and brecciated quartz-(muscovite-fluorite) veins and hydrolytic alteration, the presence of muscovite, which is a typical mineral formed in acidic conditions (Stringham 1957), also indicates progressive decrease of pH and increase of fO_2 conditions (Fig. 9).

The precipitation of chalcopyrite, the main ore mineral, was late in relation to the succession of the hydrothermal alteration stages characterized in the deposit. The first generation of chalcopyrite accompanied intense chlorite alteration, simultaneous to mylonitization, and silicification. However, expressive formation of chalcopyrite was identified in deformed quartz-(muscovite-fluorite) veins, where chalcopyrite infills fractures. Thus, chalcopyrite formation was mainly related to vein brecciation under brittle conditions. Such conditions also prevailed in undeformed milky quartz veins and in epidote-potassium feldspar veinlets with well-developed open-space filling textures. These textures are typical of ore deposition at

temperatures below 250°C, because at higher temperatures and pressures host rocks have fewer voids (Seward & Barnes 1997).

Thus, the paragenetic evolution of the Bacuri deposit points to changes of physico-chemical parameters, such as temperature decrease from 500 to 400°C (scapolite alteration) to below 250°C (late mineralized veins), accompanied by decrease of salinity and pH and increase of fO_2. However, oxidation and pH decrease unlikely caused deposition of metals transported as chloride complexes (Seward & Barnes 1997). Otherwise, decreasing temperature and salinity would be particularly effective for depositing metal in this scenario.

In the Bacuri deposit, the evolution of the hydrothermal system reflects a major change in fluid conditions. Early alteration stages (albite, scapolite-magnetite, and biotite-scapolite-magnetite alteration) developed at high temperatures due to circulation of metalliferous and hypersaline fluids. The onset of ore deposition mineralization was possibly triggered by the mixing of hypersaline, hot, metalliferous fluids and highly channelled diluted and cooler fluids within the fault zone.

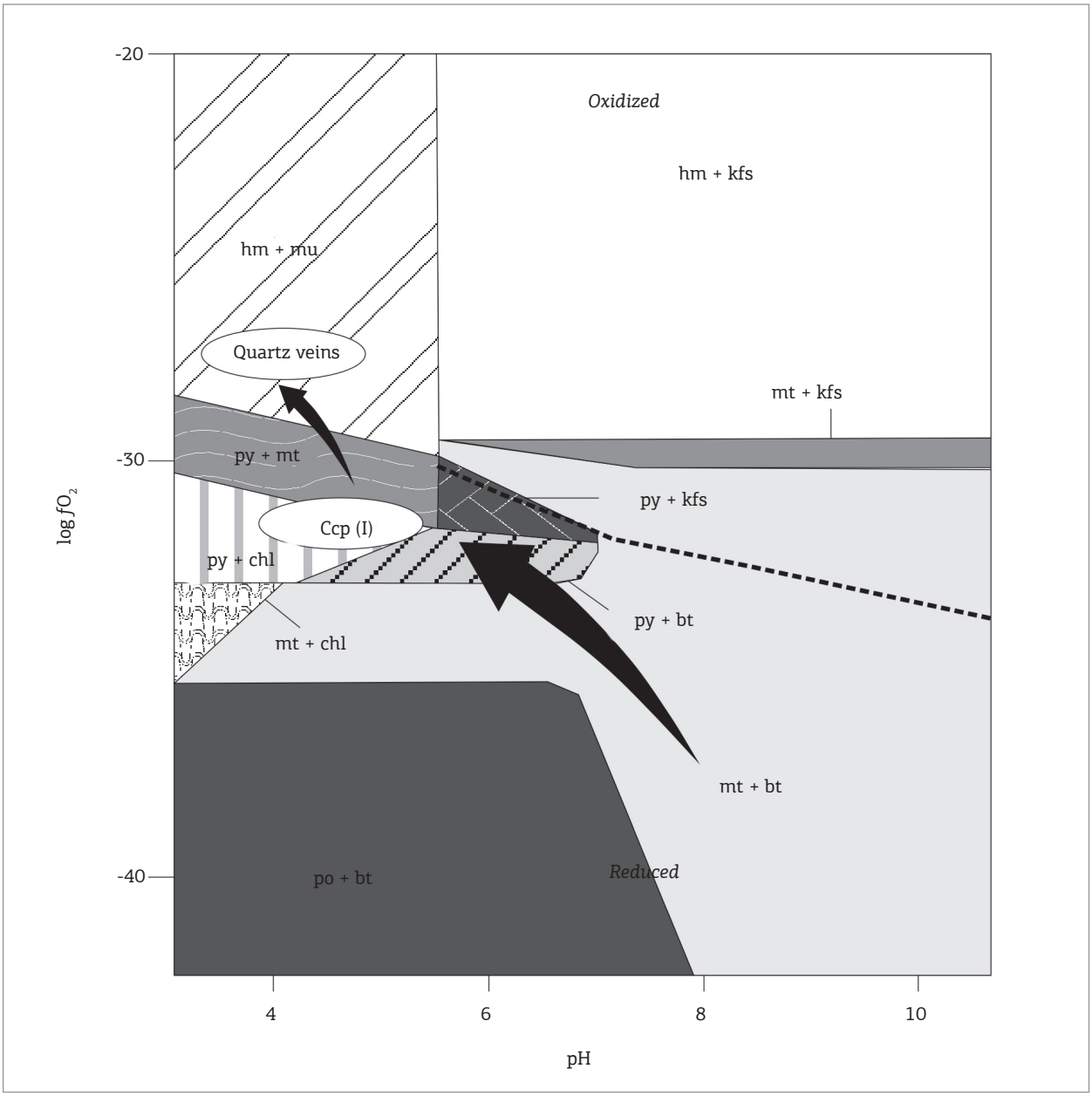

Figure 9. Diagram of pH *versus* fO_2, a 300°C, 1.5 kbar and aK+ = 0.1, showing the possible evolution of pH and oxygen fugacity of the mineralising fluid (arrow) from the initial stages (reduced conditions) to late stages (oxidized conditions) in paragenesis with the copper ore.

Transition from ductile-brittle to predominantly brittle conditions, indicated by open-space textures in late veins, could indicate progressive exhumation of the hydrothermal system.

The Bacuri deposit shares similarities with other deposits in the Carajás Province. Albite, scapolite and biotite-scapolite alteration were also previously recognized the IOCG deposits located within the regional ESE-WNW Canaã shear zone, in the southern contact between the basement rocks (e.g. 2.84 Ga Serra Dourada granite) and the 2.76 – 2.73 Ga Itacaiúnas Supergroup, such as the Pista orebody (Sossego deposit; Villas *et al*. 2005), Serra Dourada area (Sousa 2007), Bacaba, Castanha, Jatobá and Visconde deposits in Carajás (Augusto *et al.* 2008; Monteiro *et al*. 2011; Pestilho 2011; Craveiro *et al*. 2012). Thus, scapolite alteration could be considered particularly notable in the Neoarchean IOCG deposits of the Carajás Province, pointing to regional circulation of hypersaline fluids. In other major provinces that include world-class IOCG deposits, such as the Fennoscandian Shield, in Sweden (Frietsch *et al.* 1997; Smith *et al*. 2009) and Finland (Niiranen *et al.* 2005), Wernecke Mountains, Yukon, Canada (Hunt *et al.* 2005) and the district of Cloncurry, Queensland, Australia (Oliver *et al.* 1992), similar albite, scapolite and biotite-scapolite alteration zones have also been recognized. As predicted in the theoretical model of Hitzman *et al.* (1992), these alteration stages are typical of hydrothermal systems developed at relatively deep crustal levels.

In the Bacuri deposit, however, chlorite alteration zones and expressive silicification are distinct from those alteration patterns typical of others IOCG deposits in the Carajás Province. These alteration stages may record structurally controlled influx of externally derived fluids in the system coeval with the development of the NE-SW fault, overprinting the deeper regional IOCG hydrothermal system controlled by the regional ESE-WNW Canaã shear zone.

CONCLUSIONS

Detailed characterization of host rocks and hydrothermal alteration patterns carried out in this study provided insights for the evolution of the Bacuri deposit, such as:

- The Serra Dourada granite, Bacuri Porphyry, and gabbro dikes represent the host rocks of the deposit and are variably mylonitised and hydrothermally altered;
- The Bacuri deposit is located within the regional ESE-WNW Canaã shear zone, but is specially controlled by a NE-SW subsidiary fault zone;
- Spatial and temporal zoning in the Bacuri deposit suggest that hydrothermal alteration was developed due to multiple fluid pulses;
- The hydrothermal alteration sequence of the Bacuri deposit encompasses early incipient sodic (albite) alteration, scapolite-magnetite, pervasive potassic alteration with potassium feldspar, and intense biotite-scapolite-magnetite alteration. These early alteration processes are identified mainly in distal zones and may be intrinsically related to the regional migration of deep-seated hypersaline and hot metalliferous fluids within the regional ESE-WNW Canaã shear zone at relatively deep crustal levels.
- Overprinting of proximal chlorite alteration and silicification resulted from significant influx of diluted fluids within the NE-SW subsidiary fault zone, which represented an effective fluid pathway.
- Brecciation and late veins with open-space filling textures indicate progressive exhumation of the hydrothermal system.
- The paragenetic evolution of the Bacuri deposit points to changes of physico-chemical parameters, such as temperature decrease from 500 to 400°C (scapolite alteration) to below 250°C (late mineralized veins), accompanied by decrease of salinity and pH and increase of fO_2.
- The copper ore occurs disseminated in replacement zones, in small lenses, veins and breccias and is related to (i) chlorite-(epidote) alteration zones or confined in (ii) brecciated quartz-(muscovite-fluorite) veins; (iii) milky quartz veins and (iv) late potassic feldspar-epidote veinlets. Ore paragenesis includes primarily chalcopyrite, pyrite, magnetite and minor melonite, altaite, galena and cheralite associated with apatite, monazite, epidote, allanite, tourmaline, potassium feldspar, chlorite and andradite.
- The Bacuri deposit evolution points to (i) regional circulation within faults of hot hypersaline fluids that transport metals as chlorinated complexes; (ii) intense fluid–rock interaction resulting in highly modified lithotypes; (iii) mechanisms of ore deposition related to fluid mixing, which possibly triggered copper deposition via temperature decrease and dilution (decrease in a Cl^-).

ACKNOWLEDGMENTS

We thank Vale (a global mining company), particularly to Márcio Godoy and Benevides Aires, for the continuous support during field activities in the Carajás region, and to Prof. Davis Carvalho (UFPA – Vale/FAPESPA Grant). We also thank Lydia Lobato and Gema Olivo, whose comments greatly improved the manuscript. This research was funded by CNPq (472549/2009-0 and 481969/2013-6), FAPESP (2003/11163-6 and 2004/08126-4) and INCT GEOCIAM (CNPq/MCT/FAPESPA).

REFERENCES

Augusto R.A., Monteiro L.V.S., Xavier R.P., Souza Filho C.R. 2008. Zonas de Alteração hidrotermal e paragêneses do minério cuprífero do Alvo Bacaba, Província Mineral de Carajás. *Revista Brasileira de Geociências*, **38**(2):263–277.

Chiaradia M., Banks D., Cliff R., Marschik R., de Haller A. 2006. Origin of fluids in iron oxide-copper-gold deposits: Constraints from $\delta^{37}Cl$, $^{87}Sr/^{86}Sr$ and Cl/Br. *Mineralium Deposita*, **41**:565–573.

Craveiro G.S., Villas N.R., Silva A.R.C. 2012. Depósito de Cu-Au Visconde, Carajás (PA): geologia e alteração hidrotermal das rochas encaixantes. *Revista Brasileira de Geociências,* **42**:453–470.

Dardenne M.A., Schobbenhaus C.S. 2001. *Metalogênese do Brasil*. Editora Universidade de Brasília/CNPq, Brasília, 392 p.

DOCEGEO 1988. Revisão litoestratigráfica da Província Mineral de Carajás – litoestratigrafia e principais depósitos minerais. *In:* SBG, Congresso Brasileiro de Geologia, 35, Anexo aos anais, p. 11–54.

Feio G.R.L., Dall'Agnol R., Dantas E.L., Macambira M.J.B., Santos J.O.S., Althoff F.J., Soares J.E.B. 2013. Archean granitoid magmatism in the Canaã dos Carajás area: Implications for crustal evolution of the Carajás province, Amazonian craton, Brazil. *Precambriam Research*, **227**: 157–185.

Figueiredo e Silva R.C., Hagemann S., Lobato L.M., Rosière C.A., Banks D.A., Davidson G.J., Vennemann T., Hergt J. 2013. Hydrothermal fluid processes and evolution of the giant Serra Norte jaspilite-hosted iron ore deposits, Carajás mineral province. *Economic Geology*, **108**:739–779.

Fournier R.O. 1983. Active hydrothermal systems as analogues of fossil systems: In: Eaton, G., (eds.). *The Role of Heat in the Development of Energy and Mineral Resources in the Northern Basin and Range Province.* Geothermal Resources Council Special Report No. 13, p. 263–284.

Frietsch R., Tuisku P., Martinsson O., Perdahl J.-A. 1997. Early Proterozoic Cu-(Au) and Fe ore deposits associated with regional Na–Cl metasomatism in northern Fennoscandia. *Ore Geology Reviews,* **12**:1–34.

Hirata W.K., Rigon J.C., Kadekaru K., Cordeiro A.A.C., Meireles E.A. 1982. Geologia Regional da Província Mineral de Carajás. *In:* SBG/NO, Anais I, Simpósio de Geologia da Amazônia 1, p. 100–110.

Hitzman M.W., Oreskes N., Einaudi M.T. 1992. Geological characteristics and tectonic setting of Proterozoic iron oxide (Cu-U-Au-REE) deposits. *Precambrian Research,* **58**:241–287.

Huhn S.R.B., Souza C.I.J., Albuquerque M.C., Leal E.D., Brustolin V. 1999. Descoberta do depósito Cu-(Au) Cristalino: Geologia e mineralização associada região da Serra do Rabo-Carajás, PA. *In:* Simpósio de Geologia da Amazônia, 6, p. 140–143.

Hunt J., Baker T., Thorkelson D. 2005. Regional-scale Proterozoic IOCG-mineralized breccia systems: examples from the Wernecke Mountains, Yukon, Canada. *Mineralium Deposita,* **40**:492–514.

Lancaster Oliveira J., Fanton J., Almeida A.J., Leveille R.A., Vieira S. 2000. Discovery and geology of the Sossego copper–gold deposit, Carajás district, Pará State, Brazil. *In:* 31th International Geological Congress, Rio de Janeiro, *Anais* [CD-ROM].

Lindenmayer Z.G. 2003. Depósito de Cu–Au do Salobo, Serra dos Carajás: Uma revisão. In: Ronchi L.H. & Althoff F.J. (eds.), *Caracterização e modelamento de depósitos minerais*. São Leopoldo, Unisinos, p. 69–98.

Machado N., Lindenmayer D.H., Krough T.E., Lindenmayer Z.G. 1991. U–Pb geochronology of Archean magmatism and basement reactivation in the Carajás area, Amazon Shield, Brazil. *Precambrian Research,* **49**:1–26.

Melo G.H.C., Monteiro L.V.S., Xavier R.P., Santiago E.S.B., Santos A.F.F., Torres A., Aires B. 2013. A new outlook on the giant Salobo IOCG deposit: A Mesoarchean basement-hosted deposit, Carajás province. *In:* Simpósio de Geologia da Amazônia, Belém, *Anais* [CD-ROM].

Monteiro L.V.S., Xavier R.P., Hitzman M.W., Carvalho E.R., Johnson C.A., Souza Filho C.R., Torresi I. 2008a. Spatial and temporal zoning of hydrothermal alteration and mineralization in the Sossego iron oxide copper gold deposit, Carajás mineral province, Brazil: Paragenesis and stable isotope constraints. *Mineralium Deposita*, **43**:129–159.

Monteiro L.V.S., Xavier R.P., Hitzman M.W., Juliani C., Souza Filho C.R., Carvalho E.R. 2008b. Mineral chemistry of ore and hydrothermal alteration at the Sossego iron oxide–copper–gold deposit, Carajás mineral province, Brazil. *Ore Geology Reviews*, **34**:317–336.

Monteiro L.V.S., Xavier R.P., Pestilho A.L.S., Moreto C.P.N., Juliani C., Torresi I., Souza Filho C.R. 2011. O Cinturão Sul do Cobre na Província Mineral de Carajás: reconstituição do paleossistema hidrotermal associado aos depósitos de óxido de ferro–cobre–ouro. In: Frantz J.C., Marques J.C., Jost H. (Org.). *Contribuições à Metalogenia do Brasil*. Porto Alegre, UFRGS/Instituto de Geociências, v. 1, p. 41–70.

Mora C.I., Valley J.W. 1989. Halogen-rich scapolite and biotite: Implications for metamorphic fluid–rock interactions. *American Mineralogist*, **74**:721–737.

Moreto C.P.N. 2013. *U–Pb and re–os geochronology applied to the metallogenetic evolution of the Southern Copper Belt of the Carajás province* PhD Thesis, Universidade Estadual de Campinas, Campinas, 216 p.

Moreto C.P.N., Monteiro L.V.S., Xavier R.P., Amaral W.S., Santos T.J.S., Juliani C., Souza Filho C.R. 2011. Mesoarchean (3.0 and 2.86 Ga) host rocks of the iron oxide-Cu-Au Bacaba deposit, Carajás Mineral Province: U-Pb geochronology and metallogenetic implications. *Mineralium Deposita*, **46**: 789-811.

Mougeot R., Respaut J.P., Briqueu L., Ledru P., Milesi J.P., Macambira M.J.B., Huhn S.B. 1996. Geochronological constrains for the age of the Águas Claras Formation (Carajás province, Pará, Brazil). *In*: SBG, Congresso Brasileiro de Geologia 39, *Anais*, Salvador, 6, p. 579-581.

Niiranen T. 2005. *Iron oxide–copper–gold deposits in Finland: case studies from the Peräpohja schist belt and the Central Lapland greenstone belt*. PhD Thesis, University of Helsinki.

Nogueira A.C.R. 1995. *Análise faciológica e aspectos estruturais da Formação Águas Claras, Região Central da Serra dos Carajás, Pará*. Dissertação de Mestrado, UFPA, Belém, 167 p.

Oliver N.H.S., Wall V.J., Cartwright I. 1992. Internal control of fluid compositions in amphibolite-facies scapolitic calc-silicates, Mary Kathleen, Australia. *Mineralium Deposita*, **111**:94–112.

Pestilho A.L.S. 2011. *Sistemática de isótopos estáveis aplicada à caracterização da evolução dos paleo-sistemas hidrotermais associados aos depósitos cupríferos Alvo Bacaba e Alvo Castanha, Província Mineral de Carajás, PA*. MS Dissertation, Universidade Estadual de Campinas, Campinas.

Pidgeon R.T., Macambira M.J.B., Lafon J.M. 2000. Th–U–Pb isotopic systems and internal structures of complex zircons from an enderbite from the Pium Complex, Carajás province, Brazil: Evidence for the ages of granulite facies metamorphism and the protolith of the enderbite. *Chemical Geology*, **166**:159–171.

Pinheiro, R.V.L. 2013. Carajás, Brazil – A short tectonic review. *In:* Simpósio de Geologia da Amazônia, Belém, *Anais* [CD-ROM].

Reed M.H. 1997. *Hydrothermal alteration and its relationship to ore fluid composition*. In: Barnes H.L. (ed.), *Geochemistry of Hydrothermal Ore Deposits*, Wiley, New York, p. 303–365.

Réquia K., Stein H., Fontboté L., Chiaradia M. 2003. Re–Os and Pb–Pb geochronology of the Archean Salobo iron oxide copper–gold deposit, Carajás mineral province, northern Brazil. *Mineralium Deposita,* **38**:727–738.

Ribeiro A.A. 2008. *Litogeoquímica e geologia isotópica estável (C, S, O) do Depósito Cupro-aurífero do Alvo Cristalino Sul, Província Mineral de Carajás, Pará.* MS Dissertation, Universidade Federal de Ouro Preto, Ouro Preto, 127 p.

Rigon J.C., Munaro P., Santos L.A., Nascimento J.A.S., Barreira C.F. 2000. Alvo 118 copper–gold deposit: Geology and mineralization, Serra dos Carajás, Pará, Brazil. *In:* International Geological Congress, 31, Rio de Janeiro [CD-ROM].

Rimstidt J.D. 1997. Gangue mineral transport and deposition. In: Barnes H.L. (ed.), *Geochemistry of Hydrothermal Ore Deposits*, 3rd ed., New York, Wiley, p. 435–487.

Santos, J.O.S., Hartmann, L.A., Gaudette, H.E., Groves, D.I., McNaughton, N.J., Fletcher, I.R. 2000. A new understanding of the Amazon Craton Provinces based on integration of field mapping and U–Pb and Sm–Nd geochronology. *Gondwana Research*, **3**:453-488.

Sardinha A.S., Barros C.E.M., Krymsky M. 2006. Geology, geochemistry and U–Pb geochronology of the Archean (2.74 Ga) Serra do Rabo granite stocks, Carajás metalogenetic province, northern Brazil. *Journal of South America Earth Sciences*, **20**:327–339.

Seward T.M., Barnes H.L. 1997. Metal transportation by hydrothermal fluids. In: Barnes H.L. (ed.), *Geochemistry of Hydrothermal Ore Deposits*, 3rd ed, New York, Wiley, p. 435–486.

Silva M.G., Teixeira J.B.G., Pimentel M.M., Vasconcelos P.M., Arielo A., Rocha W.J.S.F. 2005. Geologia e mineralizações de Fe–Cu–Au do Alvo GT46 (Igarapé Cinzento, Carajás). *In:* Marini O.J., Queiroz E.T., Ramos B.W. (eds.), *Caracterização de Depósitos Minerais em Distritos Mineiros da Amazônia*. DNPM-CT-Mineral-FINEP-ADIMB, p. 94–151.

Smith M.P., Storey C.D., Jeffries T.E., Ryan C. 2009. In situ U–Pb and trace element analysis of accessory minerals in the Kiruna district, Norrbotten, Sweden: New constraints on the timing and origin of mineralization. *Journal of Petrology*, **50**:2063–2094.

Sousa F.D.S. 2007. *Estudo da alteração hidrotermal, com ênfase no metassomatismo sódico, de rochas granitóides e máficas da região de Canaã de Carajás, Província Mineral de Carajás, MS Dissertation,* Universidade Federal do Pará.

Souza S.R.B., Macambira M.J.B., Sheller T. 1996. Novos dados geocronológicos para os granitos deformados do Rio Itacaiúnas (Serra dos Carajás, PA): implicações estratigráficas. Simpósio de Geologia da Amazônia, 5, *Belém, Proceedings*, p. 380–383.

Stringham B. 1952. Fields of formation of some common hydrothermal-alteration minerals. *Economic Geology*, **47**:661–664.

Tallarico F.H.B. 2003. *O cinturão cupro-aurífero de Carajás, Brasil*, PhD Thesis, Universidade Estadual de Campinas, 229 p.

Tallarico F.H.B., Figueiredo B.R., Groves D.I., Kositcin N., McNaughton N.J., Fletcher I.R., Rego J.L. 2005. Geology and SHRIMP U–Pb geochronology of the Igarapé Bahia Deposit, Carajás copper–gold belt, Brazil, an Archean (2.57 Ga) example of iron-oxide Cu–Au–(U-REE) mineralization. *Economic Geology*, **100**:7–28.

Tassinari C.C.G. 1996. O mapa geocronológico do Cráton Amazônico no Brasil: revisão dos dados isotópicos. Tese de Livre Docência, Universidade de São Paulo, 139 p.

Tassinari C.C.G., Macambira M.J.B. 1999. Geochronological provinces of the Amazonian Craton. *Episodes*, **22**:174–182.

Teixeira, W., Tassinari, C.C.G., Cordani, U.G., Kawashita, K. 1989. A review of the geochronological of the Amazonian Craton: tectonic implications. *Precambriam Research*, **42**: 213-227.

Torresi I., Bortholoto D.F.A., Xavier R.P, Monteiro L.V.S. 2012. Hydrothermal alteration, fluid inclusions and stable isotope systematics of the Alvo 118 iron oxide–copper–gold deposit, Carajás mineral province (Brazil): Implications for ore genesis. *Mineralium Deposita*, **47**:299–323.

VALE 2009. *Report on the Bacuri Prospect*. Internal report (Unpublished).

VALE 2012. *Internal Report on the Bacuri*. Vale obtains operation license for Salobo. Available from: http://saladeimprensa.vale.com/en/release/interna.asp?id=22000. Cited 2013 February 4.

Vanko D.A., Bishop F.C. 1982. Occurrence and origin of marialitic scapolite in the Humboldtt Lopolith, N.W. Nevada. *Contributions to Mineral Petrology*, **81**:277–289.

Vasquez L.V., Rosa-Costa L.R., Silva C.G., Ricci P.F., Barbosa J.O., Klein E.L., Lopes E.S., Macambira E.B., Chaves C.L., Carvalho J.M., Oliveira J.G., Anjos G.C., Silva H.R. 2008. Geologia e Recursos Minerais do Estado do Pará: Sistema de Informações Geográficas – SIG: Texto Explicativo dos Mapas Geológico e Tectônico e de Recursos Minerais do Estado do Pará, 1:1.000.000. CPRM, Belém.

Villas R.N. & Santos M.D. 2001. Gold deposits of the Carajás mineral province: Deposit types and metallogenesis. *Mineralium Deposita*, **36**:300–331.

Villas R.N, Lima L.F.O., Neves M.P., Sousa F.D.S., Lamarão C.N., Fanton J., Morais R. 2005. Relações entre deformação, alteração hidrotermal e mineralização no depósito Cu–Au do Sossego, Província Mineral de Carajás. *In*: Simpósio Brasileiro de Metalogenia, 1, Gramado, RS. *Short papers* [CD-ROM].

Williams P.J., Barton M.B., Johnson D.A., Fontboté L., Haller A., Mark G., Oliver N.H., Marschik R. 2005. Iron oxide copper–gold deposits: Geology, space–time distribution, and possible modes of origin. *Economic Geology*, 100th anniversary volume, p. 371–405.

Wirth K.R., Gibbs A.K., Olszewski W.J.Jr. 1986. U–Pb ages of zircons from the Grão Pará Group and Serra dos Carajás granite, Pará, Brasil. *Revista Brasileira de Geociências*, **16**:195–200.

Xavier R.P., Monteiro L.V.S., Moreto C.P.N., Pestilho A.L.S., Melo G.H.C., Silva M.A.D., Aires B., Ribeiro C., Silva F.H.F. 2012. The iron oxide copper–gold systems of the Carajás mineral province, Brazil. In: *Geology and Genesis of Major Copper Deposits and Districts of the World: A Tribute to Richard Sillitoe*. Special Publication, Society of Economic Geologists.

Xavier R.P., Wiedenbeck M., Trumbull R.B., Dreher A.M., Monteiro L.V.S., Rhede D., Araújo C.E.G., Torresi I. 2008. Tourmaline B-isotopes fingerprint marine evaporites as the source of high-salinity ore fluids in iron oxide–copper–gold deposits, Carajás mineral province (Brazil). *Geology*, **36**(9):743–746.

Arquivo digital disponível on-line no site www.sbgeo.org.br